Trapping of Rhodamine 6G excitation energy on cellulose microparticles

Sergio G. López, Gregor Worringer,† Hernán B. Rodríguez and Enrique San Román*

Received 28th September 2009, Accepted 11th December 2009
First published as an Advance Article on the web 18th January 2010
DOI: 10.1039/b919583a

Rhodamine 6G (R6G) was adsorbed on cellulose microparticles and fluorescence quantum yields and decays were measured as a function of dye loading. Though no spectroscopic evidence of dye aggregation was found, a noticeable decrease of quantum yield—after correction for reabsorption and reemission of fluorescence—and shortening of decays were observed at the highest loadings. These effects were attributed to the dissipation of the excitation energy by traps constituted by R6G pairs, leading to static and dynamic quenching produced by direct absorption of traps and non-radiative energy transfer from monomers, respectively. Regarding the nature of traps, two extreme approaches were considered: (a) equilibrium between monomers slightly interacting in the ground state and (b) randomly distributed monomers located below a critical distance (statistical traps). Both approaches accounted quantitatively for the observed facts. The effect of energy migration was evaluated through computational simulations. As the concentration of traps could only be indirectly inferred, in some experiments an external energy transfer quencher, Methylene Blue, was coadsorbed and the results were compared with those obtained with pure R6G.

Introduction

Solid-state photosensitizers,[1] sensitized photocatalysts,[2] nanosized photoreactors,[3] solid-state lasers[4] and visible light-driven solar cells,[5] among other examples, are based on the assembly of dye molecules in heterogeneous environments. The substantial absorption of incident light currently required is achievable at high dye loadings. In these conditions, the availability of singlet excited states is strongly reduced by self-quenching unless coupling between dye and substrate assures fast deactivation of the excited dye. Strong coupling is a necessary condition to afford highly efficient charge injection into the semiconductor in sensitized photocatalysts and solar cells.[6,7] On the other hand, when the solid support is an inert material the lifetime of the singlet state must be intrinsically high. In this case, the unraveling of concentration self-quenching mechanisms becomes particularly relevant.

Reabsorption of luminescence, collisional quenching, dye aggregation and resonance energy transfer lead to concentration quenching.[8] Even when all mechanisms lead to reduced emission, their effect on the photophysical properties is quite different. Reabsorption is responsible for distortions of the emission spectrum, the decrease of fluorescence quantum yield and, if fluorescence reemission takes place, the increase in fluorescence lifetimes.[9] Reabsorption repopulates excited states, thus being advantageous for some applications. Collisional quenching resulting from molecular diffusion does affect the excited state population and results in a decrease of the emission lifetime. However, entrapping of dyes currently slows down molecular diffusion, thus precluding collisional quenching. Dye aggregation is responsible for static quenching.[10] Resonance energy transfer to energy traps results in a decrease of emission quantum yield and lifetime. Dye aggregates,[11] excimers and statistical pairs resulting from a random distribution of dye molecules[12] can act as excitation energy traps by exchange interactions or other deactivation mechanisms.

The distributions of statistical traps and free monomers are correlated with each other[13] and their concentrations cannot be varied at will. The same happens with monomers and dimers of the same species, which may be apportioned only if the dimerization constant is known. As a current assumption, a random distribution of traps is considered but its validity can hardly be demonstrated unless the donor and the acceptor are independent species.

Inner filter effects are difficult to quantify and obscure the evaluation of other concentration quenching mechanisms. Encapsulation of dyes into vesicles leads currently to very high local concentrations at a low overall absorbance, thus reducing fluorescence reabsorption.[14] However, the multiplicity of environments commonly found in vesicles renders the analysis quite difficult. Concentration self-quenching has been studied in thin films[15–17] devoid of reabsorption but the evaluation of absolute fluorescence quantum yields is usually not performed due to difficulties in establishing absorbed photon fluxes. Moreover, at high dye concentrations reabsorption is not always completely suppressed and distortions in absorption and emission spectra can be easily misinterpreted.[18]

INQUIMAE/DQIAyQF, Facultad de Ciencias Exactas y Naturales, UBA, Ciudad Universitaria, Pab. II, C1428EHA Buenos Aires, Argentina. E-mail: esr@qi.fcen.uba.ar; Fax: +54 11 4576 3341; Tel: +54 11 4576 3378
† Present address: Universität Karlsruhe (TH), Engler-Bunte-Institut, Section of Fuel Chemistry and Technology, Engler-Bunte-Ring 1, 76131 Karlsruhe, Germany

Much work has been performed in Langmuir-Blodgett films following the fluorescence decay after picosecond excitation.[19–22] Among them, Ballet *et al.* carried out a comprehensive study on multilayers of Rhodamine B substituted with octadecyl chains mixed at different ratios with film forming amphiphiles.[22] They demonstrate that global analysis is mandatory for the recovery of meaningful parameters. Sound results were obtained by the addition of a Förster-type decay and an exponential term arising from isolated dye molecules not undergoing energy transfer. The same lifetime was consistently considered for the Förster and the exponential terms. A similar decay function was used by other authors allowing different lifetime values.[23] Though the presence of aggregates as energy traps is currently considered, their concentration and its relationship to the dye analytical concentration are rarely evaluated. When statistical traps are introduced, no speculation on their nature is made. In particular, no estimation is given about the distance at which two slightly interacting dye molecules may become a trap. Furthermore, most papers neglect the possible contribution of energy migration and random distribution of traps is overall assumed.

In the present work, the effect of energy trapping in Rhodamine 6G (R6G) adsorbed on microcrystalline cellulose is studied at high local concentrations using thick layers of particles showing negligible transmission. Though this procedure apparently adds complexity as compared with experiments in solution, dilute nanoparticle suspensions or thin films, fluorescence quantum yields can be accurately calculated[24,25] and reabsorption and reemission processes can be easily accounted for.[26] Thus, the study of the remaining quenching mechanisms can be performed. In order to evaluate closely the excitation energy trapping process, an external energy transfer quencher, Methylene Blue (MB), is added in some experiments.

Experimental

Chemicals and preparation of samples

Laser grade R6G (Kodak) and MB (Fluka) were used as received after checking spectroscopically their purity. Analytical grade ethanol (Carlo Erba), methanol and diethyl-ether (Cicarelli) were used without further purification. Water was deionized and 0.22 μm-filtered in a Millipore-Q system.

Microcrystalline cellulose powder (Aldrich, average particle size 20 μm) was used as the solid support. To reduce impurities causing residual absorption and fluorescence in the visible, the solid was washed in a series of solvents (water, 1 : 1 water–methanol, methanol, 1 : 1 methanol : diethylether and diethylether), stirring 2 h and filtering after each step. The solid was finally vacuum dried during 24 h at 40 °C.

Cellulose (1 g) was suspended in R6G ethanol solutions (20 mL), the solvent was evaporated in a rotary evaporator at 40 °C during *ca.* 20 min, and samples were dried during 24 h. Evaporation time was kept nearly constant to ensure identical swelling, hence identical adsorption conditions. R6G–MB solid samples were prepared in two steps following the already described protocol: (1) R6G was adsorbed on cellulose (13 g) and the solid was dried, (2) different amounts of MB were adsorbed to identical masses of the modified solid. This procedure ensured that all samples contained the same amount of R6G and different concentrations of MB. All samples were dried at 40 °C in a vacuum oven for at least 24 h after preparation and prior to every measurement. All measurements were performed at (25 ± 2) °C.

Reflectance and emission measurements

Total and diffuse reflectance spectra of optically thick solid layers (3 mm thickness) were recorded on a Shimadzu UV-3101 scanning spectrophotometer equipped with an integrating sphere, using barium sulfate as reference. True reflectance spectra and observed fluorescence quantum yields of R6G samples were calculated from reflectance measurements with and without a suitable optical filter (Schott BG18, 2 mm thickness) in front of the detector.[24] Remission (Kubelka-Munk) functions were obtained from true diffuse reflectances as $F(R) = (1 - R)^2/2R$.[27]

Steady-state emission spectra of optically thick and thin layers of particles were obtained in front face on a PTI Model QM-1 spectrofluorometer. Thin layers were prepared spreading small amounts of powder on one side of a two-sided sticky tape fixed on a glass plate. The emission beam was passed through suitable filters (Schott OG530 or OG515, 2 mm-thickness). Spectra were corrected for changes in the detector responsivity and filter transmittance with wavelength.

R6G fluorescence decays were recorded in front face for thin layers of particles on a PTI TimeMaster fluorescence lifetime spectrometer using a medium pressure hydrogen arc lamp (R6G samples) and on a Horiba Jobin Yvon model Fluorocube fluorescence lifetime spectrofluorometer using a 495 nm LED as the excitation source (R6G–MB samples). Suitable filters were located between the sample and the detector to block scattered light.

Results and discussion

Rhodamine 6G adsorbed on cellulose

Normalized remission function spectra of selected samples are shown in Fig. 1. Absorption maxima are located at (536 ± 2) nm, 4–8 nm red-shifted and somewhat widened in comparison with the spectrum in ethanol due to differences in micro-polarity and site heterogeneity, respectively. Remission function maxima are plotted as a function of dye concentration in the inset of Fig. 1. A linear dependence of $F(R)$ with loading is found at the absorption maximum (see inset) with the exception of the most concentrated sample. The low reflectance ($R < 0.1$) may be the cause of this deviation. Data plotted at the shoulder (500 nm) show linear behavior at all loadings. Thus, no evidence on ground state aggregation is found. Interactions between dye molecules and with the solid support are weak enough to preserve the form of the spectrum.

Normalized thick layer emission spectra are shown in Fig. 2. On increasing the dye concentration, spectra show increasing red shifts (λ_{max} = 559–572 nm) and a shoulder appears at the highest wavelengths (Fig. 2a)—typical signs of fluorescence reabsorption. Once corrected for reabsorption according to

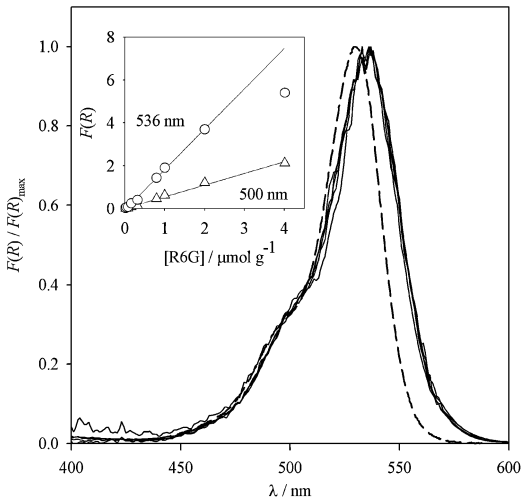

Fig. 1 Normalized remission function spectra of samples with 0.159 to 2.00 μmol g^{-1} R6G (solid lines) and absorption spectrum of R6G in ethanol (dashed line). Inset: remission function *vs.* dye concentration.

ref. 26, the spectra agree in shape with the spectrum in ethanol (λ_{max} = 551 nm, not shown) (Fig. 2b). However, a small concentration dependent red shift remains (λ_{max} = 551–557 nm) due to the interaction of the excited state with ground state neighbor molecules.[28] Very good agreement is found between corrected thick layer and thin layer spectra up to 1.00 μmol g^{-1} (not shown). Deviations found at higher concentrations show that some remaining reabsorption is still present in strongly absorbing thin layers.

Absolute fluorescence quantum yields calculated between 500 and 550 nm were corrected for reabsorption and reemission,[26,29] leading to the true fluorescence quantum yields, Φ, shown in Table 1.‡ A nearly constant quantum yield, Φ = 0.92 ± 0.03, similar to that found in ethanol solution, is found up to R6G 0.32 μmol g^{-1}. At higher loadings, concentration quenching is observed.

At R6G loadings below 2.00 μmol g^{-1}, fluorescence decays measured on thin samples are monoexponential. Lifetimes shown in Table 1 are somewhat lower than the value found in ethanol solution. For the two most concentrated samples a complex behavior is found; the monoexponential fit of the decay tail yields lower values (see Table 1), pointing again to the occurrence of concentration quenching. This effect cannot be ascribed to reemission of fluorescence by thin layers, as a lifetime increase would be expected in that case.

The above evidence demonstrates the existence of energy trapping as concentration increases. Traps must be composed by interacting dye monomers. Irrespective of their exact nature, they might be excited by direct absorption, leading to static quenching, or through energy transfer from isolated dye molecules, leading to a reduction of fluorescence lifetimes. Long range (Förster) energy transfer from dye monomers to a two-dimensional random distribution of traps will be assumed. As a first approximation, energy migration among monomers

‡ It should be recalled that Φ is a system rather than a molecular property, as it is defined as the ratio between the number of photons emitted by the monomer and the number of photons absorbed by the sample (monomers + traps).

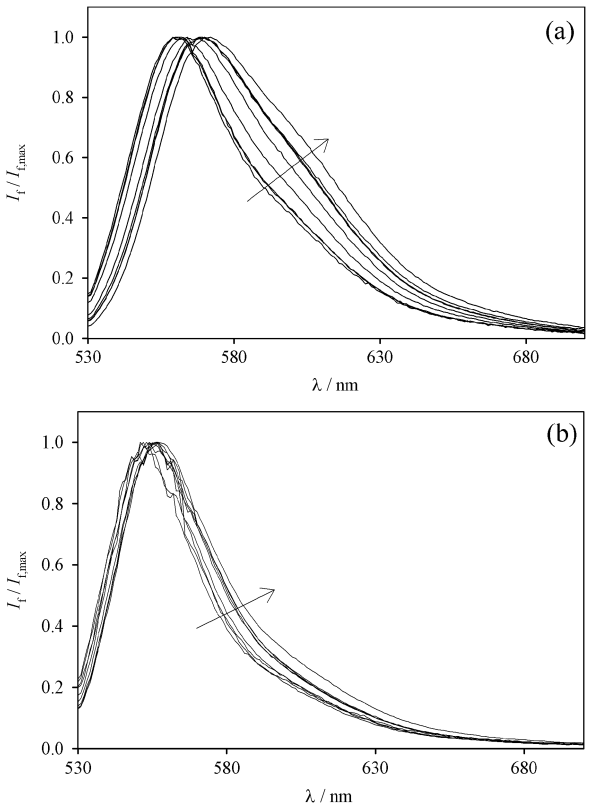

Fig. 2 Normalized R6G thick layer emission spectra (λ_{ex} = 490 nm): (a) measured, (b) corrected for reabsorption. Arrows indicate increasing loading.

Table 1 R6G adsorbed on cellulose

[R6G]/μmol g^{-1}	Φ^a	τ/ns[b]
0.021	0.89 ± 0.05	—
0.042	0.92 ± 0.02	—
0.079	0.98 ± 0.02	—
0.159	0.90 ± 0.02	3.41 ± 0.33
0.32	0.91 ± 0.02	—
0.80	0.86 ± 0.01	3.22 ± 0.08
1.00	0.79 ± 0.01	3.20 ± 0.10
2.00	0.66 ± 0.01	(2.98 ± 0.06)
4.00	0.53 ± 0.01	(2.78 ± 0.04)
R6G in ethanol[c]	0.95 ± 0.01	3.99 ± 0.03

[a] λ_{ex} = 500–550 nm. [b] Monoexponential fit of the decay tail (see text). [c] Ref. 30.

will be disregarded and non-fluorescing (perfect) energy traps will be considered. Based on these assumptions,[28,31] the monomer fluorescence decay in the presence of traps can be expressed as:

$$\frac{I(t)}{I(0)} = \exp(-x - \Gamma(2/3)\ (\delta/\delta_0)\ x^{1/3}) \qquad (1)$$

where $x = t/\tau$, τ being the monomer lifetime in the absence of traps; Γ is the gamma function; δ is the trap surface density, and $\delta_0 = 1/\pi R_0^2$, where R_0 is the Förster critical distance for energy transfer between monomers and traps.

The energy transfer efficiency can be obtained by integration of eqn (1):

$$E = 1 - \int_0^\infty \exp(-x - \Gamma(2/3)\ (\delta/\delta_0)\ x^{1/3})\mathrm{d}x \qquad (2)$$

and compared with experimental efficiencies obtained from diffuse reflectance and fluorescence data:[32,33]

$$E = 1 - \frac{\Phi}{\alpha_{0\mathrm{M}}\Phi_\mathrm{M}} \qquad (3)$$

where Φ is the sample true fluorescence quantum yield as given in Table 1,‡ Φ_M is the fluorescence quantum yield of the monomer in the absence of traps (the infinite dilution limit of Φ, estimated as 0.92, see above), and α_{0M} is the fraction of absorbed radiation exciting the monomer. Any absorption of the supporting material and any source of fluorescence other than the excited monomer are neglected. Derivation of eqn (3) is straightforward as, within the foregoing assumptions, Φ/α_{0M} is the monomer quantum yield, *i.e.* the ratio between the number of photons emitted and absorbed by the monomer, in the presence of traps.

The model eqn (2) depends on a single parameter, $(\delta/\delta_0) = \pi R_0^2\delta$. Its evaluation relies on different assumptions, which will be detailed in what follows.

(a) Evaluation of the dye surface density. The extent of swelling of the matrix, and accordingly the cellulose surface area, depends on the solvent used for the preparation of samples. The surface area is needed to calculate the dye surface density in terms of the dye loading given in μmol g^{-1}. In previous studies, a value around 60 m^2 g^{-1} was found for different dyes adsorbed from ethanol.[34] This value is assumed to hold in the present case.

(b) The spectrum of the traps is needed to calculate R_0 and α_{0M}. Within the dye concentration range used in the present work no spectral changes are observed in the absorption spectrum. This is in line with the low aggregation tendency of R6G in alcohols.[35] A slight exciton interaction between monomers will lead to imperceptible changes in the absorption spectrum and, therefore, it will be assumed that monomers and traps share the same spectrum. Therefore, α_{0M} is equivalent to the molar fraction of the dye in the isolated, monomeric state.

(c) The Förster radius was calculated as $R_0 = 51$ Å under assumption (b), considering an orientational parameter $\kappa^2 = 0.476$ (randomly distributed orientations fixed in time) and a refraction index $n = 1.47$ (glycerol). As the absorption spectrum is known through remission function data up to an unknown proportionality constant, it was scaled to the R6G spectrum in ethanol assuming equal oscillator strengths. The value reported in ethylene glycol solution is $R_0 = (55.0 \pm 0.2)$ Å.[36] The difference is ascribed mainly to changes in the spectral width and the Stokes shift on adsorption.

(d) Two extreme situations will be considered for the calculation of trap densities, differing in the driving force for trap formation. (i) If the ground state interaction between monomers is negligible and trapping takes place when monomers are closer than a certain critical distance, r_Q, assuming Poisson distribution the fraction of monomers conforming statistical traps is:

$$\frac{2\delta}{\sigma} = 1 - \exp(-\pi\ r_Q^2\sigma) \qquad (4)$$

where σ is the overall dye concentration. Only dimeric traps are considered, leading to an error lower than 5% in the trap concentration at the highest loading. (ii) If ground state interactions exist, an equilibrium approach leads to:

$$K = \frac{\delta}{(\sigma - 2\delta)^2} \qquad (5)$$

In both cases, the fraction of monomeric dye is:

$$\alpha_{0M} = 1 - \frac{2\delta}{\sigma} \qquad (6)$$

The ratio Φ/Φ_M is calculated through eqn (2) and (3) and compared with the experimental results, using r_Q or K as fitting parameters depending on the approach considered. Very good agreement is obtained for $r_Q = (15 \pm 1)$ Å and $K = (4.5 \pm 0.5)$ nm^2 (see Fig. 3). In more conventional units, after division by the surface area and multiplication by the Avogadro number, $K = (0.045 \pm 0.005)$ g μmol^{-1}. The estimated quenching radius is in the order of the molecular dimensions.[37] The value of K is consistent with the low aggregation tendency found for R6G on cellulose. A very good fitting is also obtained considering a three dimensional distribution of dyes (not shown).

The model applied so far neglects energy migration, which might have a significant effect at high donor to acceptor ratios, enhancing energy transfer efficiencies.[38,39] To account for the possible effect of energy migration on excitation energy trapping, computer simulations were performed using a Markovian model adapted from ref. 40. Details are given in the Appendix. The same R_0 was used for monomer–monomer and monomer–trap energy transfer. 2D simulations were performed but 3D trials were also run to compare with results predicted by the LAF (three-body approximation) theory.[39,41] An excellent agreement was found at a monomer concentration of up to 1×10^{-2} M (not shown). Once the simulation algorithm was tested, computational simulations were run on R6G results. The equilibrium constant and the quenching

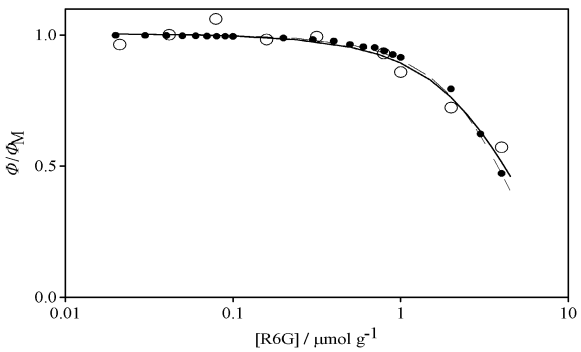

Fig. 3 Φ/Φ_M as a function of R6G loading: open circles, experimental results; solid line, dimerization approach, $K = 0.045$ g μmol^{-1}; dashed line, statistical pair approach, $r_Q = 15$ Å; circles, simulations including migration, dimerization approach, $K = 0.03$ g μmol^{-1}.

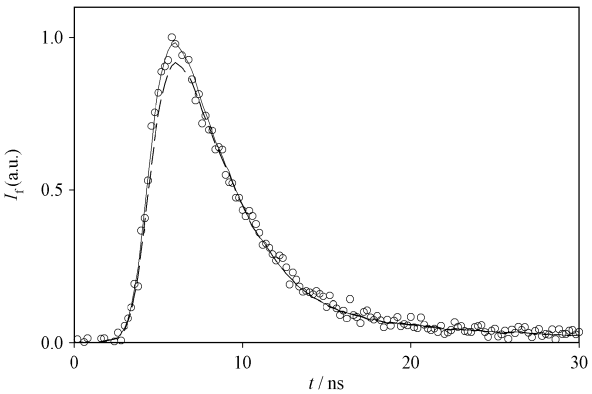

Fig. 4 Fluorescence decay for R6G 4.00 μmol g^{-1}: open circles, experimental results; solid line, convolution, dimerization approach, K = 0.045 g μmol^{-1}, τ = 3.2 ns; dashed line, convolution, mono-exponential decay, τ = 2.8 ns.

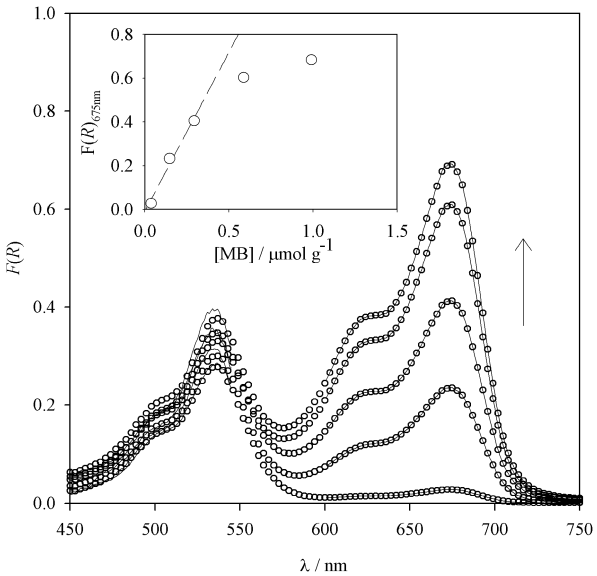

Fig. 5 Remission function spectra of R6G–MB samples, MB 0 to 0.99 μmol g^{-1}: full lines, experimental; open circles, reconstructed (see text). The arrow indicates increasing MB loading. Inset: remission function at the MB absorption maximum *vs.* MB loading.

radius were systematically varied to fit experimental data. The results obtained were $K \sim 0.03$ g μmol^{-1} (see Fig. 3) and $r_Q \sim 12$ Å (not shown). These values are quite similar to those predicted by the simplified model, showing that energy migration has only a slight effect on energy trapping in the present conditions.

Fluorescence decay curves for the last three samples (see Table 1) were convoluted with the excitation pulse, considering eqn (1) with τ and $I(0)$ as fitting parameters. The trap surface density was calculated using the dimerization approach. Excellent agreement is obtained, as shown in Fig. 4 for R6G 4.00 μmol g^{-1}. Similar results were obtained for the remaining samples. Best fits were obtained for τ = 3.2 ns.

The results obtained so far show that Förster energy transfer may be invoked to explain concentration quenching at high local R6G concentrations under the assumption of random distribution of statistical or dimeric traps. However, trap concentrations must be inferred, as they cannot be calculated *a priori*. Moreover, the concentration of R6G, and thus the concentration of traps, is restricted to the range where the Kubelka-Munk theory can be applied.

Rhodamine 6G and Methylene Blue coadsorbed on cellulose

Energy traps can be simulated through the addition of an external acceptor, whose concentration does not depend on the donor. The donor concentration can be maintained at a low value, avoiding quite low reflectances and reducing the probability of energy migration. In this way, higher quenching efficiencies may be reached and analyzed through the model eqn (1) and (2). MB was selected as the energy acceptor. Though it does not constitute a perfect trap, as MB monomers are fluorescent on cellulose with $\Phi = 0.18 \pm 0.03$,[32] the probability of back energy transfer is minimal due to the low overlap between MB emission and R6G absorption. Samples containing 0.32 μmol g^{-1} R6G and 0–1 μmol g^{-1} MB were prepared. As shown in Table 1, no self-trapping takes place at this R6G loading and any reduction of R6G fluorescence quantum yield and lifetime should be ascribed to the presence of MB.

Remission function spectra are shown in Fig. 5. As shown in the inset, in the range 0–0.29 μmol g^{-1} the remission function at the MB absorption maximum, 675 nm, is proportional to the analytical concentration. The apparent absorption coefficient of MB monomers, $F(R)$/[MB], is 1.41 g μmol^{-1}, similar to the value obtained for pure MB on cellulose, 1.44 g μmol^{-1}.[32] Deviations at higher concentrations can be ascribed to MB aggregation. Using the relative absorption coefficients of MB monomer and dimer at 675 nm,[32] the fraction of monomers involved in dimer formation can be roughly estimated as 0.29 and 0.54 for the most concentrated samples.

Due to the high R6G fluorescence quantum yield, the remission function spectrum was obtained between 400 and 545 nm from fluorescence corrected reflectances (see Experimental section). From 600 to 800 nm no fluorescence correction was performed, as only MB absorption takes place and the observed fluorescence quantum yield of MB is low. In the intermediate region, from 545 to 600 nm, where both spectra overlap and cannot be corrected for R6G fluorescence, spectra were reconstructed on the grounds of pure R6G and MB spectra, taking into account the MB dimer spectrum[32] for the most concentrated samples.

Thick layer emission spectra corrected for reabsorption are shown in Fig. 6. Excitation was performed at 500 nm, where MB does not absorb. An important decrease in R6G emission is found around 560 nm on increasing the MB loading, while a new band around 690 nm appears, near the MB emission maximum. As MB is not directly excited, R6G fluorescence quenching and increasing MB emission are evidences of energy transfer from R6G to MB. The decrease in emission intensity at large concentrations shown in the inset of Fig. 6 reflects the existence of non-fluorescent MB dimers. R6G fluorescence decays (not shown) become faster and deviate from

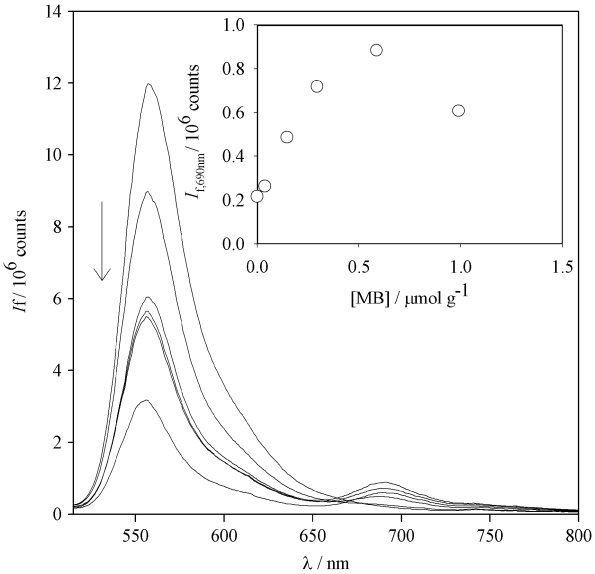

Fig. 6 Corrected R6G–MB thick layer emission spectra (λ_{ex} = 500 nm). Inset: fluorescence intensity at MB emission maximum *vs.* MB loading. The arrow indicates increasing MB loading.

Table 2 R6G–MB mixed samples on cellulose

[MB]/μmol g^{-1}[a]	τ/ns[b]
0.00	3.30
0.04	3.19
0.15	3.08
0.29	2.97
0.59	2.97
0.99	2.53

[a] R6G 0.32 μmol g^{-1}. [b] Monoexponential fit of the decay tail (see text).

monoexponential behavior on increasing the concentration of MB, showing that a non-radiative energy transfer mechanism operates. Monoexponential fits of the decay tail yielded the apparent lifetimes shown in Table 2.

Non-radiative energy transfer efficiencies were obtained from the ratio between the fluorescence intensity of R6G in thick layers of R6G–MB samples and a reference sample containing pure R6G at the same concentration:[32,33]

$$\frac{I_{F,D}}{I^*_{F,D}} = \frac{(1-R)\alpha_{0D}}{(1-R^*)\alpha^*_{0D}} \frac{(1-\Phi_D P^*_{DD})(1-E)}{[1-\Phi_D(1-E)P_{DD}]} \qquad (7)$$

where $I_{F,D}$ is the donor fluorescence intensity (560 nm), R is the total reflectance of the sample at the excitation wavelength (500 nm), Φ_D is the donor fluorescence quantum yield (0.92), α_{0D} is the fraction of the absorbed radiation exciting the donor, and P_{DD} is the probability that the donor fluorescence is reabsorbed by the donor.[32] Superscript * indicates absence of quencher (MB). All quantities can be accessed through remission function and fluorescence data.

Energy transfer efficiencies obtained from eqn (7) are shown in Fig. 7 together with values calculated through eqn (2) assuming a surface area of 60 m^2 g^{-1} and a Förster radius of 49 Å for the energy transfer from R6G to MB monomers.

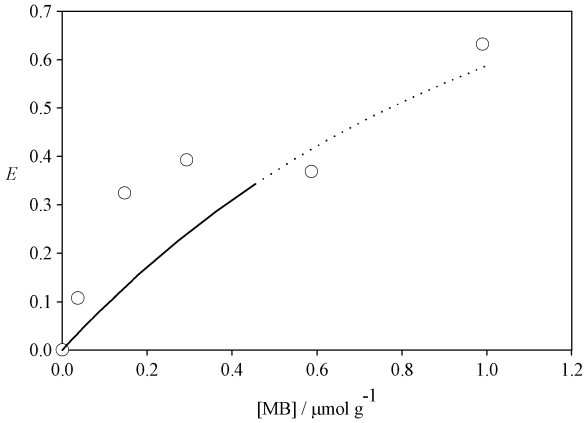

Fig. 7 R6G quenching efficiencies *vs.* MB loading: open circles, experimental results, eqn (7); dashed line, calculated through eqn (2).

To evaluate the Förster overlap integral, the area under the remission function spectrum of MB on cellulose was scaled to the absorption spectrum measured in ethanol. As a first approximation, MB aggregation was not taken into account in the calculations.

Fig. 7 shows that E values obtained from eqn (7) are noticeably higher than those calculated with eqn (2) at concentrations at which MB is monomeric. Scaling the area under the remission function spectrum of MB dimers on cellulose to the monomer absorption spectrum in the same medium, the Förster radius for energy transfer from R6G to MB dimers can be estimated as 51 Å, slightly higher than the monomer–monomer Förster radius. In spite of that, theoretical efficiencies considering dimerization would be lower due to the decrease in acceptor concentrations, hence widening the gap between experimental and theoretical values.

The model leading to eqn (7) has been validated under quite different conditions.[34] Therefore, the discrepancy between experimental and theoretical E values found at the lower concentrations indicates that either the magnitude of the selected parameters or the validity of the assumptions leading to eqn (2) is not valid. (1) Energy migration among donor molecules, which would enhance energy transfer efficiencies, can be safely excluded at the low R6G concentration used in these experiments. (2) Overestimation of the cellulose surface area would yield lower theoretical efficiencies. However, using the cellulose surface area as a fitting parameter at concentrations where MB dimerization is negligible, a value of 24 m^2 g^{-1} is obtained. This exceedingly low value is incompatible with results found for several systems prepared under almost identical conditions.[34,42] (3) The underestimation of R_0 would also yield lower theoretical efficiencies but this could hardly be the reason because estimated values are similar to those calculated for the same dyes in solution. (4) Finally, the observed differences may arise from a non-random distribution of MB (acceptor) around individual R6G (donor) molecules. The existence of hydrophobic donor–acceptor interactions will lead to shorter average distances in spite of the electrostatic repulsion due to the positive charge of both dyes, thus enhancing the energy transfer efficiency.

Comparison between R6G and R6G–MB mixed samples

Results obtained from mixed samples might be thus qualitatively explained on the grounds of a non-random distribution of acceptors arising from weak hydrophobic interactions in the hydrophilic environment provided by cellulose. The effect of interactions is quite different in Langmuir-Blodgett films.[21,22] In this case, an exponential term has to be added to account for the existence of "isolated" dye monomers and, in extreme situations, phase separation is observed. In the present case, interactions may lead to the formation of weakly bound R6G–MB complexes enhancing energy transfer. A similar phenomenon might also affect results obtained for pure R6G samples. The effect would be different, depending on the nature assumed for the traps. The equilibrium approach leads indeed to a non-random distribution of R6G molecules. In that case, excluding three-molecule interactions, short range forces will be relevant only within the monomer pair constituting the dimer and the distribution of dimeric traps around a particular donor may be considered as random. Therefore, under this assumption, the equilibrium constant K will be correctly evaluated. The low value of K supports this conclusion, since at the highest dye concentrations $<20\%$ of the dye molecules is in the dimeric state. If the same value of K is assumed for the formation of trimers from monomers and dimers, only 4% of the dye molecules would be involved. The case is quite different in the statistical pair approach. Interaction between monomers will lead to closer average distances. The result is an overestimated value of r_Q, which therefore has to be considered as an upper limit.

Conclusions

Concentration-dependent quenching of R6G fluorescence was observed after correction for reabsorption effects in pure R6G and mixed R6G–MB samples. In the former case, the distribution of monomers and traps is interdependent, while for mixed samples the acceptor concentration can be externally controlled. Concentration quenching of R6G fluorescence on cellulose microparticles is ascribed to the formation of excitation energy traps. Quenching is both static—light absorption by traps—and dynamic—energy transfer from excited monomers to traps, leading to shorter decay times. Traps may be understood as close lying dye molecules bound by hydrophobic forces. Interaction is weak enough to cause undetectable spectroscopic changes. In the present case, energy trapping requires that almost non-interacting monomers are placed at a distance of around 12–15 Å. This result can be used as a rule for the design of non-random dye arrays in which crosstalking of individual monomers is avoided, thus assuring low losses by energy trapping. Similar R6G–MB interactions can explain the departure of trapping efficiencies from the behavior predicted by the Förster theory assuming random distribution of acceptor molecules. The results are consistent with the low aggregation tendency of R6G on cellulose and with the lack of evidence on heteroaggregation in the mixed system.

Appendix

Numerical simulations

The following algorithm can be used in a space of arbitrary dimensionality. An area (volume) is defined in the 2D (3D) space and monomer 1 is located at its center. The simulation area (volume) is scaled and the rest of isolated monomers and all traps are located using a random number generation algorithm to define the molecular coordinates. The total number of donors and acceptors are calculated from the known surface densities (volumetric concentrations). The simulation space should be large enough to minimize border effects, assuring that excitation is trapped within its frontiers in the vast majority of cases. This condition is met through trial and error. Förster energy transfer among monomers and from monomers to traps is assumed.

A vector of energy transfer efficiencies is defined as follows:

$$\boldsymbol{E} = \sum_{n=0}^{\infty} (\boldsymbol{P}_{\mathbf{MM}})^n \times \boldsymbol{P}_{\mathbf{MT}} = (\boldsymbol{I} - \boldsymbol{P}_{\mathbf{MM}})^{-1} \times \boldsymbol{P}_{\mathbf{MT}} \qquad \text{(A1)}$$

whose elements are the calculated energy trapping efficiencies for every monomer in a particular run. The elements of matrix $\boldsymbol{P}_{\mathbf{MM}}$ are the probabilities p_{ij} that excitation is transferred from monomer i to monomer j, those of vector $\boldsymbol{P}_{\mathbf{MT}}$ are the probabilities p_{iT} that excitation is transferred from monomer i to any trap in the system, and $\mathbf{I}$ is the $n_M \times n_M$ unit matrix, where n_M is the number of monomers in the simulation space. The matrix $\boldsymbol{P}_{\mathbf{MM}}$ and the vector $\boldsymbol{P}_{\mathbf{MT}}$ are given by:

$$\boldsymbol{P}_{\mathbf{MM}} = \begin{pmatrix} 0 & p_{12} & \dots & p_{1n_M} \\ p_{21} & 0 & \dots & p_{2n_M} \\ \dots & \dots & \dots & \dots \\ p_{n_M1} & p_{n_M2} & \dots & 0 \end{pmatrix} \quad p_{ij} = \frac{1}{S_i}\left(\frac{R_0^{MM}}{r_{ij}}\right)^6 \qquad \text{(A2)}$$

$$\boldsymbol{P}_{\mathbf{MT}} = \begin{pmatrix} p_{1T} \\ p_{2T} \\ \dots \\ p_{n_MT} \end{pmatrix} \quad p_{iT} = \frac{1}{S_i}\sum_{t=1}^{n_T}\left(\frac{R_0^{MT}}{r_{it}}\right)^6 \qquad \text{(A3)}$$

where the summation S_i is a normalization factor, including all possible transfer steps originated from monomer i:

$$S_i = \sum_{\substack{j=1 \\ j\neq i}}^{n_M}\left(\frac{R_0^{MM}}{r_{ij}}\right)^6 + \sum_{t=1}^{n_T}\left(\frac{R_0^{MT}}{r_{it}}\right)^6 + 1 \qquad \text{(A4)}$$

In eqn (A4), all rates are referred to the intrinsic deactivation of the excited monomer, represented by "1" at the right hand side. In the above equations, $R_0{}^{MM}$ and $R_0{}^{MT}$ are the Förster radii for M–M and M–T transfer, respectively, r_{ij} is the distance between monomer i and monomer j, r_{it} is the distance between monomer i and trap t, and n_T is the number of traps in the simulation space, respectively.

The matrix product in eqn (A1) represents all possible ways into which excitation, initially located at monomer i flows into any trap in the simulation space. Only the element of vector $\boldsymbol{E}$ corresponding to the central monomer, E_1, needs to be

considered. After N simulations, the mean energy trapping efficiency is calculated as:

$$\langle E \rangle = \frac{1}{N}\sum_{k=1}^{N} E_{1k} \qquad \text{(A5)}$$

where N is the number of simulations, characterized by different monomer and trap distributions. The appropriate size of the simulation space and the number of simulations are selected through the calculation of trapping efficiencies at increasing values of both quantities, until a constant result is reached within a predefined error level. A square (cube) of side longer than $10R_0$ and $N > 1000$ were used in all cases.

Acknowledgements

Financial support from ANPCyT (PICT 00938), CONICET (PIP 319) and UBA (UBACyT X202) is gratefully acknowledged. G.W. thanks DAAD for a student fellowship in Buenos Aires. S.G.L. and H.B.R. thank CONICET for a graduate and a postgraduate fellowship, respectively. E.S.R. is a staff member of CONICET. Special thanks are due to Elizabeth Jares-Erichman and Guillermo Menéndez for helping with time-resolved measurements.

References

1 D. E. Wetzler, D. García-Fresnadillo and G. Orellana, *Phys. Chem. Chem. Phys.*, 2006, **8**, 2249–2256.
2 D. Chatterjee and S. Dasgupta, *J. Photochem. Photobiol., C*, 2005, **6**, 186–205.
3 S. Hashimoto, *J. Photochem. Photobiol., C*, 2003, **4**, 19–49.
4 E. Yariv, S. Schultheiss, T. Saraidarov and R. Reisfeld, *Opt. Mater.*, 2001, **16**, 29–38.
5 M. Grätzel, *J. Photochem. Photobiol., C*, 2003, **4**, 145–153.
6 J. B. Asbury, E. Hao, Y. Wang, H. N. Ghosh and T. Lian, *J. Phys. Chem. B*, 2001, **105**, 4545–4557.
7 D. F. Watson and G. J. Meyer, *Annu. Rev. Phys. Chem.*, 2005, **56**, 119–156.
8 Z. Petrášek and D. Phillips, *Photochem. Photobiol. Sci.*, 2003, **2**, 236–244.
9 B. Valeur, in *Molecular Fluorescence. Principles and Applications*, Wiley-VCH Verlag GmbH, Weinheim, 1st edn, 2001, ch. 4, pp. 110–112.
10 M. Kasha, H. R. Rawls and M. Ashraf El-Bayoumi, *Pure Appl. Chem.*, 1965, **11**, 371–391.
11 V. I. Yuzhakov, *Russ. Chem. Rev.*, 1992, **61**, 613–628.
12 L. G. Boulu, L. K. Patterson, J. P. Chauvet and J. J. Kozak, *J. Chem. Phys.*, 1987, **86**, 503–507.
13 J. Knoester and J. E. Van Himbergen, *J. Chem. Phys.*, 1987, **86**, 3571–3576.
14 A. L. Plant, *Photochem. Photobiol.*, 1986, **44**, 453–459.
15 A. V. Deshpande and E. B. Namdas, *J. Lumin.*, 2000, **91**, 25–31.
16 P. Bojarski, *Chem. Phys. Lett.*, 1997, **278**, 225–232.
17 P. A. Anfinrud, T. P. Causgrove and W. S. Struve, *J. Phys. Chem.*, 1986, **90**, 5887–5891.
18 P.-A. Cazade, P. Bordat, S. Blanc, I. Baraille and R. Brown, *Langmuir*, 2008, **24**, 2252–2257.
19 N. Tamai, T. Yamazaki and I. Yamazaki, *Chem. Phys. Lett.*, 1988, **147**, 25–29.
20 E. Vuorimaa, M. Ikonen and H. Lemmetyinen, *Chem. Phys.*, 1994, **188**, 289–302.
21 D. Pevenage, M. Van der Auweraer and F. C. De Schryver, *Langmuir*, 1999, **15**, 8465–8473.
22 P. Ballet, M. van der Auweraer, F. C. De Schryver, H. Lemmetyinen and E. Vuorimaa, *J. Phys. Chem.*, 1996, **100**, 13701–13715.
23 K. Kemnitz, T. Murao, I. Yamazaki, N. Nakashima and K. Yoshihara, *Chem. Phys. Lett.*, 1983, **101**, 337–340.
24 M. Mirenda, M. G. Lagorio and E. San Román, *Langmuir*, 2004, **20**, 3690–3697.
25 L. F. Vieira Ferreira, T. J. F. Branco and A. M. Botelho do Rego, *ChemPhysChem*, 2004, **5**, 1848–1854.
26 M. G. Lagorio, L. E. Dicelio, M. I. Litter and E. San Román, *J. Chem. Soc., Faraday Trans.*, 1998, **94**, 419–425.
27 W. W. Wendlandt and H. G. Hecht, in *Reflectance Spectroscopy*, Wiley Interscience, New York, 1966, ch. 3, pp. 55–76.
28 K. Itoh, Y. Chiyokawa, M. Nakao and K. Honda, *J. Am. Chem. Soc.*, 1984, **106**, 1620–1627.
29 H. B. Rodríguez, M. G. Lagorio and E. San Román, *Photochem. Photobiol. Sci.*, 2004, **3**, 674–680.
30 D. Magde, R. Wrong and P. Seybold, *Photochem. Photobiol.*, 2002, **75**, 327–334.
31 N. Nakashima, K. Yoshihara and F. Willig, *J. Chem. Phys.*, 1980, **73**, 3553–3559.
32 H. B. Rodríguez, A. Iriel and E. San Román, *Photochem. Photobiol.*, 2006, **82**, 200–207.
33 H. B. Rodríguez and E. San Román, *Ann. N. Y. Acad. Sci.*, 2008, **1130**, 247–252.
34 H. B. Rodríguez, *PhD Thesis*, University of Buenos Aires, 2009.
35 L. Malfatti, T. Kidchob, D. Aiello, R. Aiello, F. Testa and P. Innocenzi, *J. Phys. Chem. C*, 2008, **112**, 16225–16230.
36 P. Bojarski, A. Matczuk, C. Bojarski, A. Kawski, B. Kukliński, G. Zurkowska and H. Diehl, *Chem. Phys.*, 1996, **210**, 485–499.
37 N. Iyi, R. Sacia, T. Fujita, T. Deguchi, T. Sota, F. López Arbeloa and K. Kitamura, *Appl. Clay Sci.*, 2002, **22**, 125–136.
38 L. Kulak and C. Bojarski, *Chem. Phys.*, 1995, **191**, 43–66.
39 L. Kulak and C. Bojarski, *Chem. Phys.*, 1995, **191**, 67–86.
40 C. Carlsson, A. Larsson, M. Björkman, M. Jonsson and B. Albinsson, *Biopolymers*, 1997, **41**, 481–494.
41 R. F. Loring, H. C. Andersen and M. D. Fayer, *J. Chem. Phys.*, 1982, **76**, 2015–2027.
42 A. Iriel, *PhD Thesis*, University of Buenos Aires, 2006.